

Sep.2019 / Vol.167

M i t s u b i s h i E l e c t r i c

ADVANCE

Breakthroughs in Electro-optics Microwave and Communication Technologies

• **Editorial-Chief**

Tomoyuki Kobayashi

• **Editorial Advisors**

*Omi Kuriwaki
Daisuke Kashibuchi
Masayuki Sato
Hiroaki Sakai
Hiroaki Shiraki
Shinsuke Yamamoto
Yusuke Nakata
Kunihiko Egawa
Mineo Okada
Osami Kamohara
Kota Omori
Eunjin Choi
Yasuhiro Endo
Ryo Ikehara
Toshihiro Kurita*

• **Vol. 167 Feature Articles Editor**

Masataka Otsuka

• **Editorial Inquiries**

Tomoyuki Kobayashi
Corporate Total Productivity Management
& Environmental Programs
Fax: +81-3-3218-2465

Mitsubishi Electric Advance is published on line quarterly (in March, June, September, and December) by Mitsubishi Electric Corporation. Copyright © 2019 by Mitsubishi Electric Corporation; all rights reserved. Printed in Japan.

The company names and product names described herein are the trademarks or registered trademarks of the respective companies.

CONTENTS

Technical Reports

Overview 1
by *Masataka Otsuka*

Compressive Sensing Technology for Synthetic Aperture Radar 2
by *Takehiro Hoshino*

Pulsed Serrodyning Optical Transceiver Technology for Wind-Sensing Coherent Doppler Lidar 5
by *Toshiyuki Ando* and *Eisuke Haraguchi*

A Broadband Satellite Communication Technology for a Safe and Secure Society 8
by *Shigenori Tani*

Phased Array Antenna Using Directional Modulation with Sum & Difference Pattern for Secure Communication 12
by *Tasuku Kuriyama* and *Jun Goto*

Multiband Digital Transmitter Techniques Using High-Efficiency GaN Switching-Mode Amplifiers 16
by *Shintaro Shinjo* and *Rui Ma*

Precis

Mitsubishi Electric Corporation's sensing and communication technologies using light and radio waves have often led the industry and given us a business advantage. These technologies are the basis of the IoT and have recently been applied to many of our business areas in response to demands for further improvements. This issue introduces the latest development examples.

Overview



Author: *Masataka Otsuka**

Breakthroughs in Electro-Optics Microwave & Communication Technologies

Communications and sensing—mobile communications, satellite communications, wireless LAN, Fiber To The Home (FTTH), onboard information devices, home information appliances, and various radar and optical sensors—provide the foundation of the IoT society. Mitsubishi Electric Corporation's electro-optics microwave and communication technologies span a diverse range of systems and end-use hardware in both sectors and are used in many of its business areas. Our electro-optics microwave and communication technologies contain many elemental technologies, such as sensor signal processing, communications (radio and optical), optical sensors, antennas, microwave circuits, and EMC. Each technology has been advancing while involving other technologies in different sectors. This issue introduces industry-leading examples of such development.

Example combinations of technologies in the electro-optics microwave and communication sectors include array antennas for secure communications, pulsed serrodyning optical transceivers, and increased capacity of satellite communications. Example combinations of technologies in other sectors include the use of compressive sensing for synthetic aperture radar and digital transceivers using GaN switching amplifiers.

The IoT will play a key role in meeting the needs of modern society for safety, security, resilience, and sustainability. Electro-optics microwave and communication technologies, which are the foundation of this IoT, must continue to be developed in the future.

Compressive Sensing Technology for Synthetic Aperture Radar

Author: Takehiro Hoshino*

1. Introduction

Synthetic aperture radar (SAR) uses sensors installed on satellites and airplanes to monitor the ground day and night in any weather. Although SAR is suitable for observing a wide area, the observation area needs to be expanded to reduce the total observation time. To do this without affecting image quality, Mitsubishi Electric Corporation developed the "DAICHI-2" advanced land-observing satellite-2 with two radar antennas, achieving high-resolution wide swath (HRWS). However, since the number of antennas was increased to two, the amount of data to be downlinked also doubled.

Due to the data volume for HRWS, the downlink faces a shortage of capacity, so the amount of downlink data needs to be reduced. To reduce the data size, compressive sensing technology was proposed in 2006.⁽¹⁾

Mitsubishi Electric has been developing a compressive sensing technology for SAR that contributes to resource-saving space development^{(2), (3)} and has confirmed in an airplane SAR experiment that even when the data size is halved at regular intervals from the conventional size, the data can be reconstructed. This paper reports the details.

2. Compressive Sensing SAR

Figure 1 illustrates the concept of compressive sensing SAR. In compressive sensing SAR, the observable area is halved and the available extra resource is used to observe another area, thus expanding the coverage.

3. Principle of Compressive Sensing

3.1 Sampling theorem

Compressive sensing is a technology that overcomes the limit of the data size determined by the sampling theorem. The sampling theorem states that to reconstruct data of up to a certain frequency faithfully, it is sufficient to double the sampling frequency. Figure 2 shows an example where, when the sampling theorem is not satisfied, the frequencies cannot be identified. The solid line shows the true wave motion and the circles show signals observed in sampling. The broken line is wave motion (ambiguity) having a high frequency for which the observed values are the same as those in the true wave motion. Whether the solid or broken line is the

true wave motion cannot be determined only by observing the circles.

3.2 Random sampling

To solve the problem in Fig. 2, random sampling is used in compressive sensing in general. Figure 3 shows an example of random sampling. In random sampling, the solid line is distinguished from the broken line when

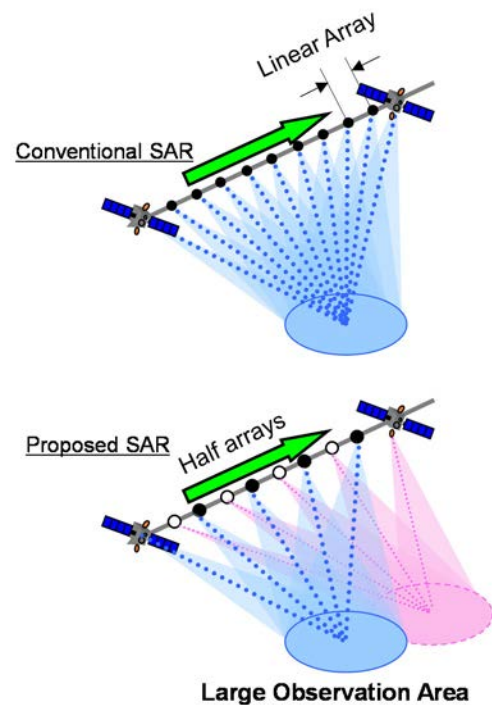


Fig. 1 Concept of compressive sensing SAR

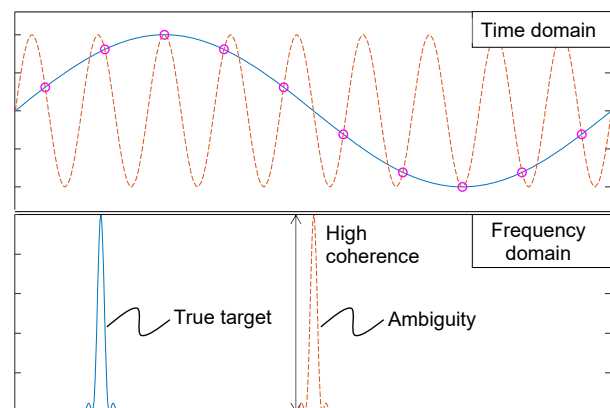


Fig. 2 Two sinusoidal waves on time/frequency domains with sub-Nyquist linear sampling

observing the circles and so it can be understood that the solid line is the true wave motion. When Fourier transform (FT) is performed on the values observed in random sampling and the frequency domain is analyzed, the high-frequency ambiguity component seen in Fig. 2 is diffused and becomes smaller. This means that the coherence of the ambiguity is reduced.

3.3 Compressive sensing for SAR

In general compressive sensing, random sampling is a solution. However, in SAR, for reflection sources away from the center of observation, changes in distance from the observation point are not even, so the radio waves change as shown by the broken line in Fig. 4 relative to the observation point. Therefore, the solid line can be distinguished from the broken line even in the case of sampling at regular intervals. This means that the coherence of the ambiguity component (broken line) is reduced and the ambiguity's intensity level after FT is lowered. In addition, the solution (SAR image) is extracted on the assumption that the solution is sparse. This is the principle of compressive sensing for SAR developed this time.

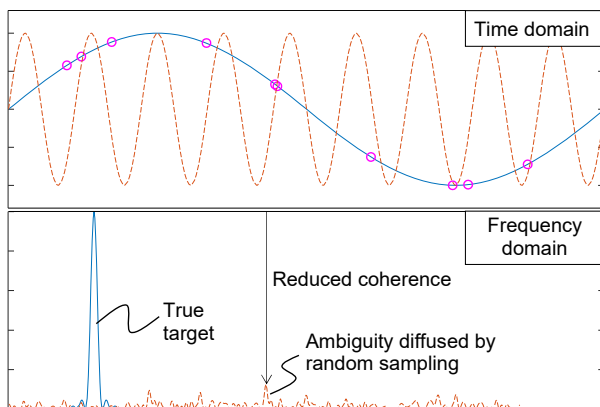


Fig. 3 Two sinusoidal waves on time/frequency domains with sub-Nyquist random sampling

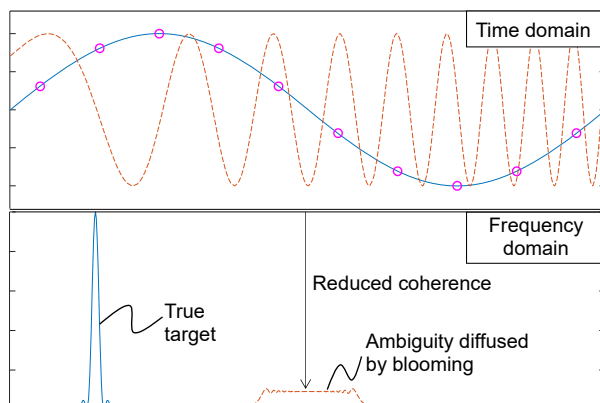


Fig. 4 Two waves of SAR observation on time/frequency domains with sub-Nyquist linear sampling

4. Verification of the Principle in a Ku-band Airplane SAR Experiment

This section studies the effect of compressive sensing for improving the level of ambiguity of a SAR image for which the data size was reduced at regular intervals. Figure 5 shows a Ku-band airplane SAR system developed by Mitsubishi Electric. The airplane was Diamond Air Service Inc.'s Gulfstream-II. Table 1 lists the experimental parameters. The sampling ratio is defined as the value obtained by dividing the pulse repetition frequency (PRF) by the Doppler bandwidth; when the ratio is 1.0 or higher, the sampling theorem is satisfied. Figure 6 shows a SAR image when the data size was reduced at regular intervals and when the sampling ratio was 0.6. Figure 7 shows the result of applying compressive sensing to the data in Fig. 6. The figure shows that compressive sensing suppressed the ambiguity (in the white box) caused by the sampling theorem no longer being satisfied due to the reduction of data size at regular intervals. Figure 8 shows a SAR image that satisfies the sampling theorem. Comparing Fig. 7 and Fig. 8, the data has been equally reconstructed thanks to the compressive sensing. The ratio of the intensity between the point with the maximum intensity among the true points composing the image and the point with the maximum intensity in the ambiguity domain is defined as the ambiguity level. Table 2 shows the evaluation results. The table shows that the ambiguity level was reduced by 9.6 dB to -45.5 dB by compressive sensing compared with -35.9 dB before its application. On the other hand, the ambiguity level of the SAR image satisfying the sampling theorem is -58.7 dB. These results show that compressive sensing could further improve the ambiguity level by 13.2 dB, indicating room for improvement.

5. Conclusion

This basic study of compressive sensing for SAR confirmed in an airplane SAR experiment that even when the data size is halved at regular intervals unlike conventional random sampling, the data can be reconstructed by the compressive sensing technology. The ambiguity level was improved by 9.6 dB. Meanwhile,

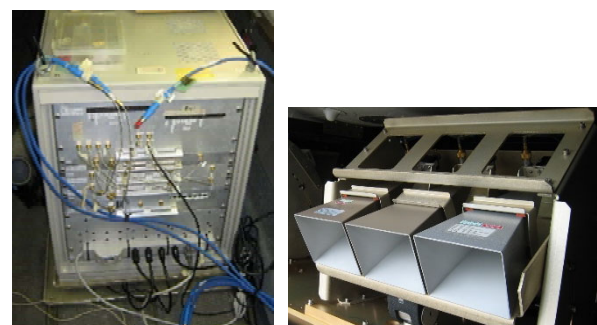


Fig. 5 Ku-band airplane SAR system

Table 1 Parameters of experimental study with airplane SAR

Center frequency	16.45 GHz
SAR image resolution	10 cm × 10 cm
Sampling ratio before reduction of data size	1.2
Sampling ratio after reduction of data size	0.6

Table 2 Evaluation of ambiguity level

SAR image with sampling ratio of 1.2	-58.7 dB
SAR image with sampling ratio of 0.6	-35.9 dB
SAR image with compressive sensing applied	-45.5 dB



Fig. 6 Half subsampled SAR imagery (sampling ratio is 0.6)



Fig. 7 Reconstructed result of Fig. 6 with proposed compressive sensing



Fig. 8 Original SAR imagery (sampling ratio is 1.2)

there is still room to improve the level by 13.2 dB. This technology is expected to be used to reduce the size and cost of SAR sensors and for other purposes, thus contributing to resource-saving space development.

6. References

- (1) Eldar, Y.C., et al., Compressed Sensing, Cambridge University Press (2012)
- (2) Liu, D., et al., Synthetic aperture imaging using a randomly steered spotlight, IEEE IGARSS, 919-922 (2013)
- (3) Hoshino, T., et al., Experimental studies of compressive sensing for SAR with Ka-band chamber room and Ku-band airplane SAR data, IEEE IGARSS, 5366-5369 (2017)

Pulsed Serrordyning Optical Transceiver Technology for Wind-Sensing Coherent Doppler Lidar

Authors: Toshiyuki Ando* and Eisuke Haraguchi**

1. Introduction

Coherent Doppler lidar (CDL) systems are attractive sensors for wind sensing because they offer a method of measuring wind speed remotely under clear atmospheric conditions. An all-fiber CDL system using a 1.5-micron wavelength has many advantages, such as compactness, eye-safety, and reliability, thanks to the use of commercial off-the-shelf components for telecoms products⁽¹⁾. The use of CDL is expanding rapidly for many wind energy applications⁽²⁾. Mitsubishi Electric released its first-generation commercial all-fiber CDL system in 2006, and the second-generation compact CDL, DIABREZZATM™, for assessing wind resources in 2014. An international standard for wind sensing with CDL was published recently⁽³⁾, which will accelerate the spread of CDL for wind sensing. However, CDL is not small enough to be transported because an acoustic optical modulator (AOM) is used in optical transmitters.

For widespread use of CDL, compactness and transportability are essential. Accordingly, we have developed a new small optical transmitter using a semiconductor optical amplifier (SOA) and a lithium niobate optical phase modulator (LNM) with saw-tooth waveform, which provides pulsed serrordyne modulation⁽⁴⁾.

2. System Configuration

Figure 1 shows a schematic block diagram and external view of the mobile coherent Doppler lidar. This new lidar has an all-in-one design consisting of an optical transceiver board directly connected with a signal processor, an optical high-power amplifier (OHPA), an optical antenna via a fiber circulator, and a lithium polymer battery. The dimensions are 39×29×16 (W×H×D) cm and the weight is 2.9 kg. The optical transceiver is combined a conventional fiber-optic heterodyning receiver with a newly developed coherent optical pulse seeder based on pulsed-serrordyne modulation. In the signal processing board a system-on-a-chip (SoC) solution has been adopted by using a large field programmable gate array (FPGA) with an internal processor core. Measured wind data can be displayed on a tablet PC via WiFi after on-board signal processing for wind speed estimation.

3. Optical Transceiver Unit

Figure 2 shows the block diagram and external view of the optical transceiver unit as a coherent pulse seeder combined with a heterodyne receiver. All fiber-optic components are commercial off-the-shelf components used for optical communication and have high reliability, being compliant with Telcordia GR468-core. An integrable tunable laser assembly (ITLA) is used as a master laser with a line width of 200 kHz and wavelength of 1550 nm. Its output is split into a local oscillator (LO) and a seed light to a pulsed serrordyne modulator which consists of a semiconductor optical amplifier (SOA), a lithium niobate optical phase modulator (LNM) and their drivers with digital-to analog converters (DAC). The pulsed serrordyne modulation is our newly developed technique to realize both pulse modulation and

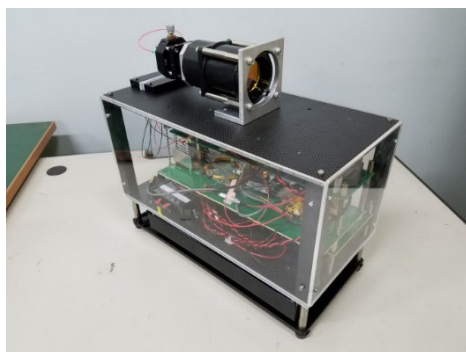
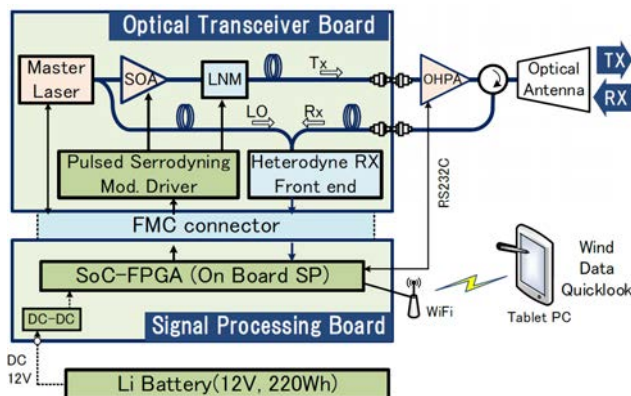


Fig. 1 Schematic block diagram and external view of the mobile Doppler lidar

frequency shift without the double-pass acousto optic (AO) modulator currently used in our CDL system [3].

In the receiver section, optical return signals (RX) are phonically mixed with a LO signal, then detected as intermediate frequency (IF) signals at two balanced photodiodes (PD). In order to accommodate a bandwidth of 100 MHz corresponding to a Doppler frequency range of ± 35 m/s, the heterodyning signal is sampled at the rate of 216 MSps with an analog-to digital converter (ADC) and transferred to the signal processing board.

4. Pulsed Serrodyning Modulator

Serrodyne frequency shifting is realized by applying saw-tooth phase modulation to the optical signals. Recently, the frequency shift of a few hundred megahertz required in CDL can be obtained with good quality by technological advances in high-speed driver electronics. Furthermore, SOA is promising for an optical pulse modulator with a small footprint if the issue of frequency chirp can be solved. We have newly developed a pulsed serrodyning modulation which realizes both frequency shift and compensation of frequency deviation in SOA⁽⁵⁾. Figure 3 shows the temporal signals of pulsed serrodyning modulation for the optical intensity of a SOA and the optical phase of an LNM. The saw-tooth phase modulation is applied within only the pulse-on period, T1, over the pulse repetition interval (PRI). If the complete

saw-tooth phase modulation with cycle of Tm is applied, the output optical frequency is shifted with an offset frequency of 1/Tm.

It is worth noting that no frequency shift occurs within the pulse-off periods because a saw-tooth signal is not applied. This leads to effective rejection of unwanted beat noise between optically internal reflections within the pulse-off periods and the LO signal in the heterodyne receiver without such a special pulsed modulator as a double-pass AOM with a high extinction ratio.

5. Experimental Results

In order to confirm whether the pulsed-serrodyning modulation works correctly, line-of-sight (LOS) wind Doppler spectra were evaluated in the case of pulsed-serrodyne modulation and that of single-pass AO modulation as a reference. The measuring conditions were as follows: a pulse-on period T1 of 500 ns corresponding to a range resolution of 75 m, a PRI of 250 μ s, a saw-tooth cycle, and Tm of 6.17 ns corresponding to IF of 162 MHz as shown in Fig. 3. Figure 4 shows the LOS wind Doppler spectra at a distance of 500 m. In the case of single-path AO modulation the spectrum has a strong peak around zero Doppler velocity which may be caused by beat noise between a LO signal and internal reflection of leaky light within the pulse-off periods. This unwanted beat noise

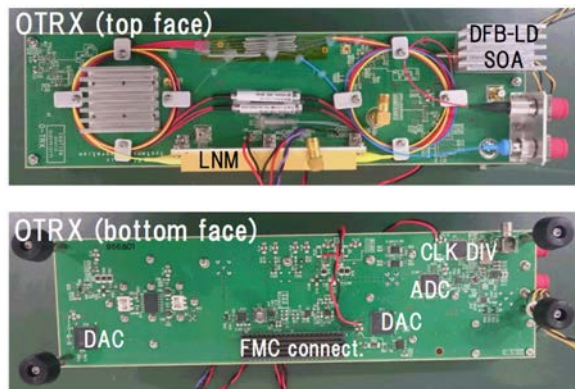
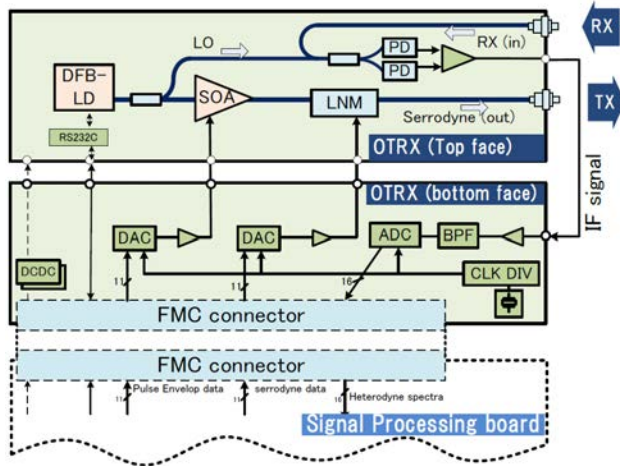


Fig. 2 Schematic block diagram and external view of the optical transceiver unit

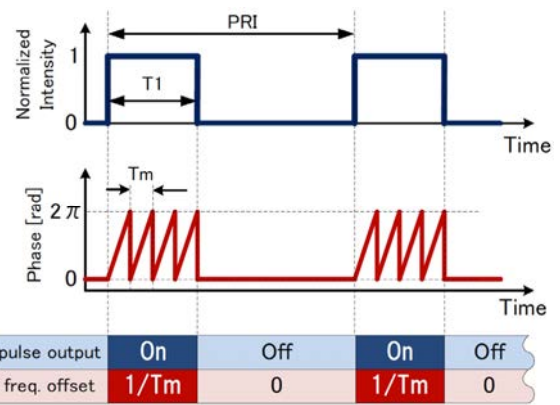


Fig. 3 Temporal signals of pulsed serrodyning modulation for the optical intensity of a SOA and the optical phase of an LNM

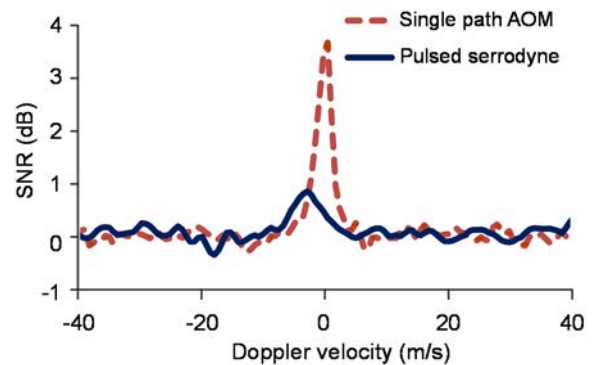


Fig 4 LOS wind Doppler spectra at distance of 500 m

makes it difficult to measure wind signals near the zero-Doppler velocity. Meanwhile, the spectrum of pulsed-serrodyne modulation has a peak at around -1 m/s without any noise peak at the zero-Doppler velocity.

Figure 5 shows the measurement data of the LOS wind velocity with respect to distance and that of their detectability. Theoretical calculation for detectability is also shown as a function of distance. The setting parameters are as follows: optical peak power of 30 W at a fiber end of an OHPA, aperture diameter of 50 mm, focusing distance of 500 m, and integration number of 4000. The back-scattering coefficient is assumed to be $8.3 \times 10^{-8} \text{ m}^{-1} \text{sr}^{-1}$ taking into account the number of aerosols measured using a particle counter.

The measured detectability closely agrees with the theoretical curve, which indicates that the LOS wind velocities are measured up to 900 m because of the larger detectability than the detection limit of 7 dB.

Figure 6 shows the temporal variation of supplying power from fully charged batteries for continuous wind sensing under the same measurement conditions as in Fig. 5. In this figure, the present mobile CDL performed wind measurements for 5 hours 20 minutes without having to replace the battery. The average supply power was 31.4 W.

6. Conclusion

We have developed a new mobile coherent Doppler lidar for wind sensing with dimensions of $39 \times 29 \times 16$ cm.

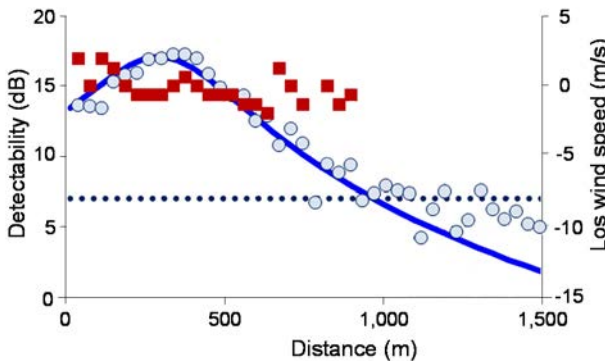


Fig 5 LOS wind velocity and detectability with respect to distance

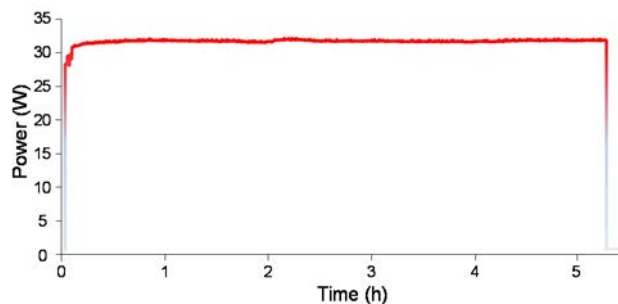


Fig 6 Battery supplying power under continuous wind sensing

Pulsed-serrodyne modulation makes it possible to realize both frequency shift and compensation of frequency chirp within the pulse-on periods of the SOA as pulse modulator. The new mobile lidar can be powered by a lithium battery and can continuously measure wind profiles for over 5 hours, thanks to the low power consumption of the optical transceiver and signal processor subsystem. Preliminary experiments have been performed by using this mobile lidar for line-of-sight wind velocities with the maximum horizontal range of more than 1 km.

7. References

- (1) S. Kameyama et al., "Compact all-fiber pulsed coherent Doppler lidar system for wind sensing," *Applied Optics*, vol. 46, 1953 (2007).
- (2) T. Mikkelsen, N. Angelou, K. Hansen, M. Sjöholm, M. Harris, C. Slinger, P. Hadley, R. Scullion, G. Ellis, and G. Vives, "A spinner-integrated wind lidar for enhanced wind turbine control," *Wind Energy*, 16, 625–643 (2012).
- (3) ISO28902-2: "Air quality-Environmental meteorology – Part 2: Ground-based remote sensing of wind by heterodyne pulsed Doppler lidar" (2017).
- (4) T. Ando et al., "New coherent Doppler lidar engine integrating optical transceiver with FPGA signal processor," *Proc. of. 18th CLRC*, 145 (2016).
- (5) E. Haraguchi et al., "Optical frequency deviation compensation using pulsed serrodyne technique on coherent laser transmitter for wind sensing lidar," *Appl. Physics Express*, vol. 12, 052006 (2019).

A Broadband Satellite Communication Technology for a Safe and Secure Society

Author: *Shigenori Tani**

1. Introduction

Frequent, high-definition observation of global-scale climate changes is important to reduce the impacts of natural disasters on people's lives. Recently, the combination of technological innovation in the space industry with information communication technologies in other industries has led to expectations for new businesses for mapping various types of information on geographic spaces to acquire new information. In such systems, a large volume of data needs to be transmitted between satellites and ground stations in near real-time. This paper describes the latest trend in technologies to increase the data capacity for earth observation satellites and communication satellites. The paper also outlines the combination of communications and observation as a vision of the future.

2. Trend in Earth Observation Satellites and Future Technologies

2.1 Trend

In recent years, in addition to more accurate sensors to be installed on earth observation satellites, constellations of multiple satellites circling in low earth orbit are expected to make earth observation possible in near real-time. Such systems require high-speed datalinks to transmit observation data quickly to ground stations.

There are two types of datalink for earth observation satellites: one via data relay satellites located in geostationary orbit and the other in which data is directly transmitted to ground stations from the satellites in low earth orbit. The propagation loss on direct transmission paths is smaller than via geostationary orbit, and high-speed transmission is possible. Conventionally, direct transmission has used the X-band (8-GHz band), but the bandwidth becomes restricting as the transmission rate is increased. Therefore, the Ka-band (26-GHz band) for which the bandwidth (1.5 GHz) is four times that of the X-band has been studied. In addition, the Q-band (39-GHz band) that can use 3 GHz of bandwidth might improve the transmission rate.

2.2 Future technologies

Using high-frequency bands such as the Ka-band and Q-band will increase the antenna gain and usable

bandwidth, and thus improve the rate of data transmission from earth observation satellites to ground stations. However, attenuation due to the atmosphere, such as rain, will also increase: when the elevation angle is low, in particular, waves travel further through the atmosphere, so the influence is large. Site diversity technologies in which multiple ground stations are used effectively improve the availability in rain. However, when the frequency band is switched to the Ka-band and Q-band from the X-band, the area of the beam transmitted from the satellite becomes smaller due to the increased frequency, so the signal to noise power ratio (SNR) in reception changes based on the positional relationship between the satellite and ground station, which is a problem. In addition, for the Q-band, earth observation satellites have been assigned as secondary users, so their interference to primary users (e.g., terrestrial networks) must be smaller than the specified value.

To solve such problems, a technique to control beams transmitted from earth observation satellites adaptively is effective.⁽¹⁾ This technique improves the reception SNR of the satellite systems and keeps the interference to terrestrial networks smaller than the specified value through adaptive control. Figure 1 illustrates an outline of this technique. First, as shown in Fig. 1(a), the satellite changes the orientation of the transmitting antenna to select site diversity or single-station reception dynamically. Next, as shown in Fig. 1(b), it changes the antenna's rotation angle such that the reception SNR becomes maximum by making the pattern of the transmitting antenna asymmetrical like an oval antenna. Lastly, as shown in Fig. 1(c), when a

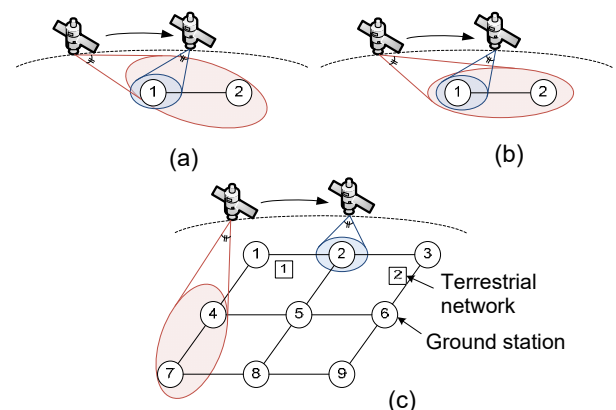


Fig. 1 An example of beam control

terrestrial network is located near the target ground station, it selects another ground station to reduce the interference. When a terrestrial network is near the target ground station, the satellite controls the beam radiation position using a weighting factor to improve either the availability or degradation of SNR preferentially. This technique improves the availability of the terrestrial networks and concurrently reduces the degradation of the SNR of the earth observation satellite system as shown in Fig. 2.

In addition, the transmittable time with a ground station is limited within the visible range where the ground station can be seen from the satellite, so observation data may need to wait to be sent if some data could not be sent within the transmittable time. To resolve this problem, the multi-carrier multi-hop communication technique shown in Fig. 3 works well. The technique improves the data transmission probability for each transmission opportunity in earth observation satellite constellations.⁽²⁾ A satellite using this technique has a channelizer and multiple transmitters. The transmitters perform encoding and modulation based on the quality of paths. The channelizer demultiplexes signals input from the transmitters to sub-channels and uses the switch to multiplex its own signals with signals from other satellites for sending to the inter-satellite-link or direct

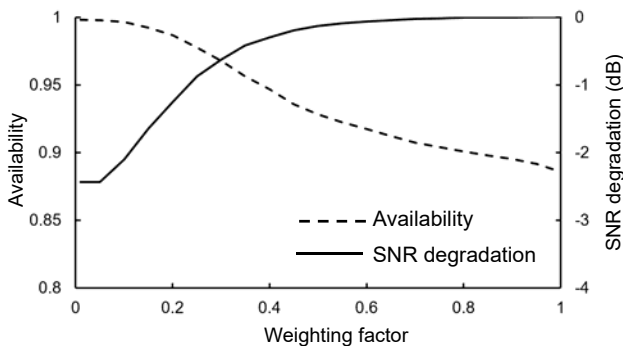


Fig. 2 Availability of terrestrial networks and SNR degradation of satellite link

transmission path. Figure 4 illustrates an example of transfer using this technique. The control station calculates the transmittable capacity for each of the satellites that can communicate with ground stations. It then selects multiple ground stations to which the earth observation satellites will send all data that they possess and determine the inter-satellite-link path to send the data to the target ground stations (routing information).

3. Trend in Communication Satellites and Future Technologies

3.1 Trend

For communication satellites, the high throughput satellite (HTS) has been used to reduce the bit cost of a single satellite. In HTS, multiple short-range beams reuse frequencies to increase the relay capacity. Figure 5 illustrates the configuration of an HTS system. A terminal is located in each of multiple beams radiated from the satellite and communicates with the gateway via the satellite. A modern HTS system has tens of beams to span cover the coverage area, achieving a channel capacity of approx. 100 Gbit/s by the entire system. As the frequency plan, the user link consists of the four-color frequency reuse scheme (two frequencies and two polarized waves). However, when multiple beams are used to span the coverage area, frequencies for the feeder link run out. As a solution, multiple gateways are provided at geographically separate locations to reuse the frequencies of the feeder link to increase the number of beams for the user link.

3.2 Future technologies

Currently, many HTS systems are bent-pipe repeaters in which the frequency of each beam and the connection between the beams are fixed. On the other hand, digital channelizers and beam hopping are effective for improving the frequency efficiency, by assigning frequencies or time flexibly based on changes in communication demand. As the speed of devices

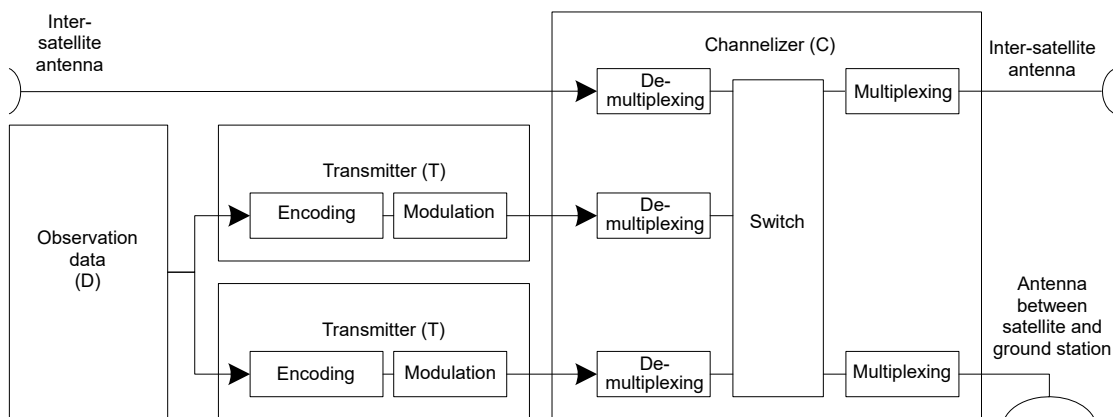


Fig. 3 Satellite function block for multi-carrier and multi-hop relaying

installed on satellites becomes higher, digital channelizers and beam hopping are expected to be applied to broadband systems (e.g., Ka-band systems). Mitsubishi Electric Corporation has developed a digital channelizer including de-multiplexing and multiplexing circuits that process up to 640 MHz per beam.

Conventionally, when a digital channelizer is used to concentrate frequencies to a specific beam, it is done

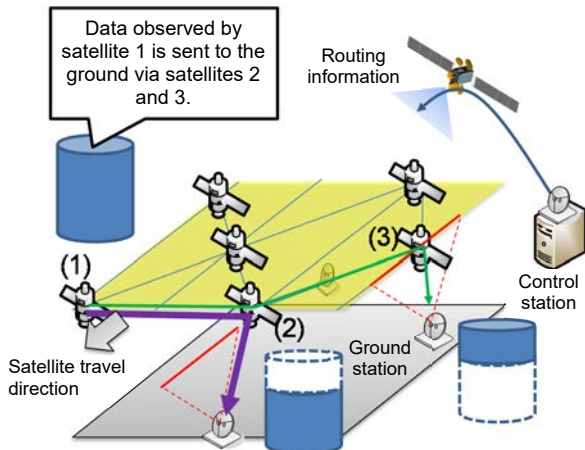


Fig 4 An example of data transfer

within the bandwidth assigned to the user link. Meanwhile, for the Ka-band, the frequency bands assigned to the user link and feeder link are continuous. Therefore, as shown in Fig. 6, by changing the ratio of the bands between the user link and feeder link, the bandwidth of the user link can be significantly increased.⁽³⁾ This technique allows the feeder link and user link to be assigned to the same frequency repeatedly by selecting a gateway that does not interfere much with the beam to which the frequency should be intensively assigned when traffic is concentrated to a specific beam, which can increase the transmission capacity as shown in Fig. 7.

In addition, for conventional beam hopping, the movable ranges (clusters) of the beams transmitted from satellites are independent, so when traffic is unbalanced between the clusters, the frequency efficiency deteriorates. To solve this problem, the overlapping clustering beam-hopping technique is effective. In this technique, the domains of the clusters overlap with each other and the beam is radiated from a different cluster to an area to which the traffic is concentrated. This

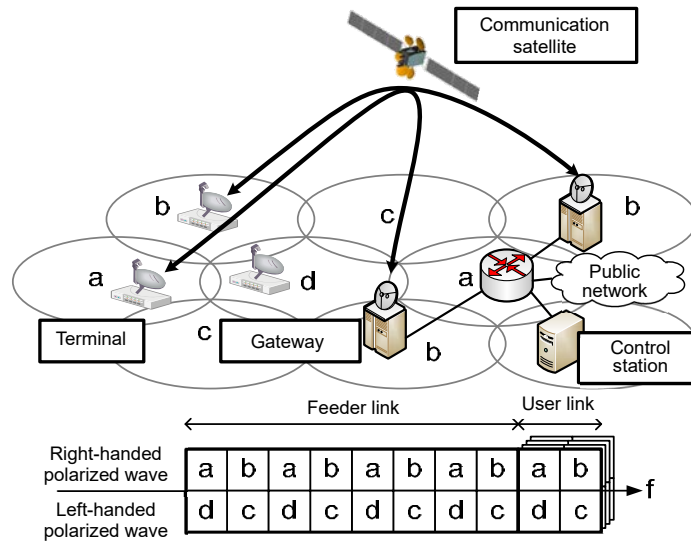


Fig 5 System architecture of HTS

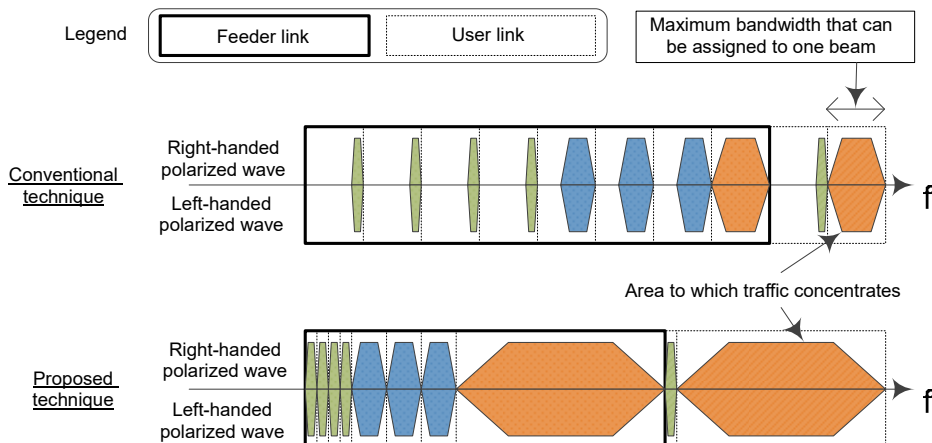


Fig 6 Comparison of frequency plan

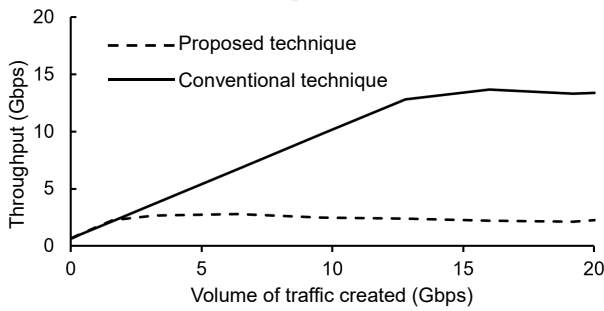


Fig 7 Throughput performance in congested area

achieved by a single system; it is important to establish scalable and flexible systems suitable for each user.

5. Conclusion

This paper described the trend in earth observation and communication satellites that support safety and security, as well as future technologies that control methods of sending data from satellites to ground stations and exchanging data between satellites based on their positional relationship and volume of data left unspent adaptively to increase the transmission capacity.

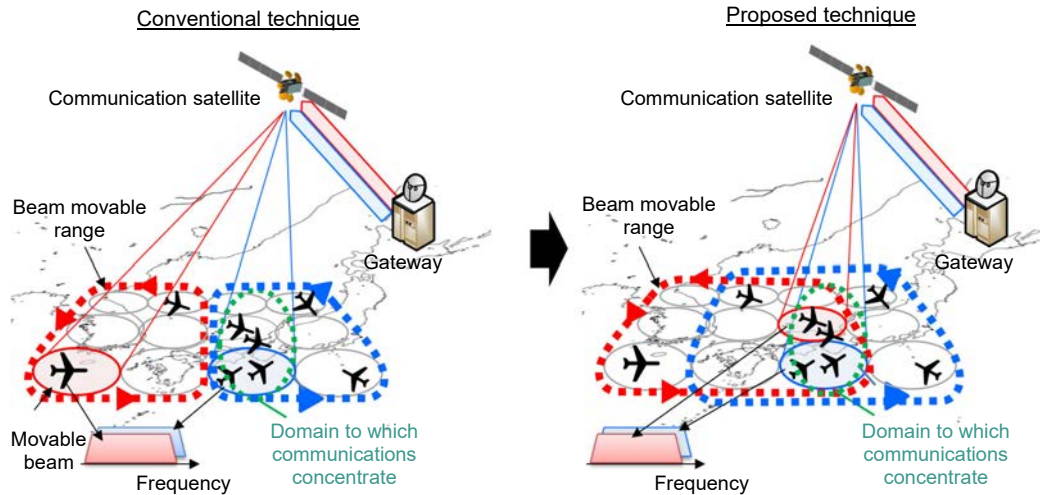


Fig 8 Overview of the overlapping clustering beam-hopping technique

technique can improve the transmission capacity to approximately 1.5 times that of the conventional technique.⁽⁴⁾

4. Combination of Observation and Communications

To reduce the impact of natural disasters on people's lives, it is important to understand the situation quickly and take action promptly. It is effective to establish real-time observation systems to understand the situation: hybrid networks in which HTS systems are combined with inter-satellite transmission that was described in the preceding part and that is used to achieve low-delay transmission are effective. Earth observation satellite systems and satellite communication systems both require higher speed, immediacy, and accommodation of multiple users. Effective ways to achieve this are broadband transmission using the Ka-band, improvement of the frequency efficiency using multiple beams, and improvement of the flexibility by satellite digital payload. Thus, both types of systems have similarities, from the configuration of the networks to single components, so systems in which observation and communications are combined using integrated networks may be established in the future. However, these services cannot be

The paper also showed the similarities between earth observation satellite and communication satellite technologies, and expectations for services that combine both types of technologies.

6. References

- (1) Tani, S., et al.: An Adaptive Beam Control Technique for Q Band Satellite to Maximize Diversity Gain and Mitigate Interference to Terrestrial Networks, IEEE Trans. on Emerging Topics in Computing (2017)
- (2) Tani, S., et al.: Multi-carrier Relaying for Successive Data Transfer in Earth Observation Satellite Constellations, IEEE Global Communications Conference (2017)
- (3) Tani, S., et al.: Flexibility-Enhanced HTS System for Disaster Management: Responding to Communication Demand Explosion in a Disaster," IEEE Trans. on Emerging Topics in Computing (2017)
- (4) Tani, S., et al.: Overlapping Clustering for Beam-hopping Systems, 36th AIAA International Communications Satellite Systems Conference, International Communications Satellite Systems Conferences (2018)

Phased Array Antenna Using Directional Modulation with Sum & Difference Pattern for Secure Communication

Authors: *Tasuku Kuriyama** and *Jun Goto**

1. Introduction

In radio communications, information is transmitted and received in open spaces using radio waves. Therefore, communication radio waves may be intercepted by unintended people and the contents may be wiretapped and decrypted. To prevent such risks, common key cryptosystems and other cryptographic techniques are widely used.

Other measures proposed by researchers include physical layer security techniques in which radio waves and signal processing are used to enhance security.⁽¹⁾ In one such technique, the channel characteristics are used to share secret keys only among legitimate users, and in another human-made noise known to legitimate users is introduced to the desired signals to prevent the signals from being noticed.⁽²⁾ This paper introduces the phased array antenna—a physical layer security technique—for which a directional modulation technology that can control the ranges in which signals can be demodulated (hereafter, “directional modulation array”) is used.

This paper reports the principle of the method to calculate the excitation distribution of directional modulation arrays and the results of evaluating the communication performance.

2. Directional Modulation Arrays

2.1 Directional modulation technologies

In the directional modulation method, carrier signals are modulated using phase shifters and variable attenuators installed on phased array antennas to form modulating signals which are then transmitted from each element antenna.⁽³⁾ By carefully designing the excitation distribution of phase shifters and variable attenuators, modulating signals radiated from each element antenna become meaningful signals only after being combined in the communication direction; in other directions they are irregular signals.

Methods to calculate the excitation distribution of phase shifters and variable attenuators that realize directional modulation have been studied. Conventionally, optimization methods using genetic

algorithms are used to calculate the excitation distribution⁽³⁾, but this makes the calculation volume large. One way to solve this problem is the sum and difference patterns synthesis method—a simple excitation distribution calculation method that does not rely on the calculation processing capability of communication systems.^{(4), (5)}

2.2 Sum and difference patterns synthesis method

Figure 1 shows the principle of the sum and difference patterns synthesis method. In the method, a desired signal beam to send the desired signals is formed at the same time with an interference signal beam to send the interference signals.

The desired signal beam is formed in a shape such that the beam pattern peak is in the communication direction. This beam pattern is called a sum pattern. On the other hand, the interference signal beam is formed in a shape such that the null of the beam pattern faces the communication direction and the gain of the interference signal beam is higher than that of the desired signal beam in other directions. The beam pattern for which the communication direction is null is called a difference pattern. By forming sum and difference patterns at the

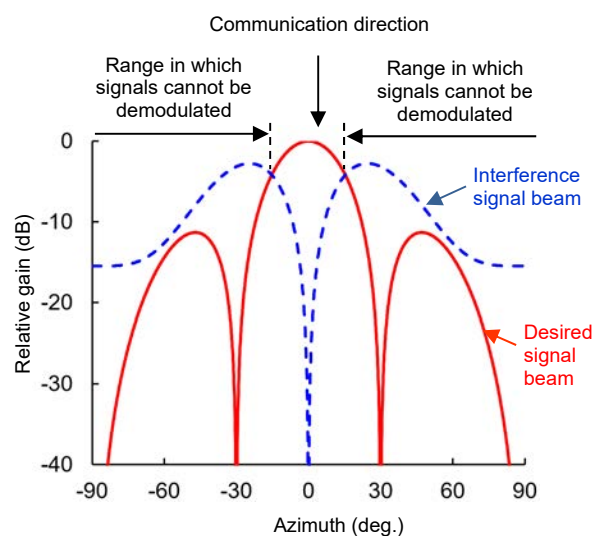


Fig. 1 Principle of sum and difference patterns synthesis method

same time, the power ratio between the desired and interference signals can be changed depending on the transmit direction and the angle width in which signals can be demodulated can be limited only near the communication direction. Specifically, desired signals are transmitted with a stronger signal power than the interference signals near the communication direction, so they can be demodulated. On the other hand, in the sidelobe direction of the desired signal beam, interference signals are transmitted with a stronger signal power than the desired signals, so the desired signals cannot be demodulated.

Figure 2 illustrates the configuration of a directional modulation array using the sum and difference patterns synthesis method. The excitation distribution which forms the desired signal beam shown in Fig. 1 is multiplied by the desired signals, and that which forms the interference signal beam is multiplied by the interference signals. They are combined to calculate the excitation distribution. Based on this excitation distribution, the phase shifter and variable attenuator control the amplitude phases of the carriers transmitted from each element antenna.

3. Evaluation of Characteristics

Table 1 lists the simulation parameters. The communication performance when a 4-element phased array antenna is used for communication in quadrature phase shift keying (QPSK) is evaluated.

3.1 Beam patterns

Figure 3 shows amplitude characteristics of the beam patterns sending QPSK symbols, and Fig. 4 shows their phase characteristics. The beam patterns were obtained by multiplying each beam shown in Fig. 1 by the desired signals or interference signals and combining in consideration of phase values. The legends in Figs. 3 and 4 indicate the phase value of each QPSK symbol. The four types of beam pattern shown in the figures are switched according to desired signals. When focusing on the amplitude phase in the communication direction with the azimuth of 0 degrees, the amplitude is equal amplitude for each symbol as shown in Fig. 3 and the phase values are 45, 135, -135, and -45 degrees as shown in Fig. 4. They match the QPSK constellation. Figure 5 shows the constellations received in the communication direction (0-degree direction) and a direction other than the communication direction (30-degree direction). This figure shows the amplitude phase value of each azimuth in Figs. 3 and 4 on the complex plane. As shown in the figure, the constellation in the communication direction is that of QPSK, but in the direction (30-degree direction) other than the communication direction, the symbol points concentrate to a point and are disordered. Thus, the directional modulation technology can allow constellations to have angular dependence.

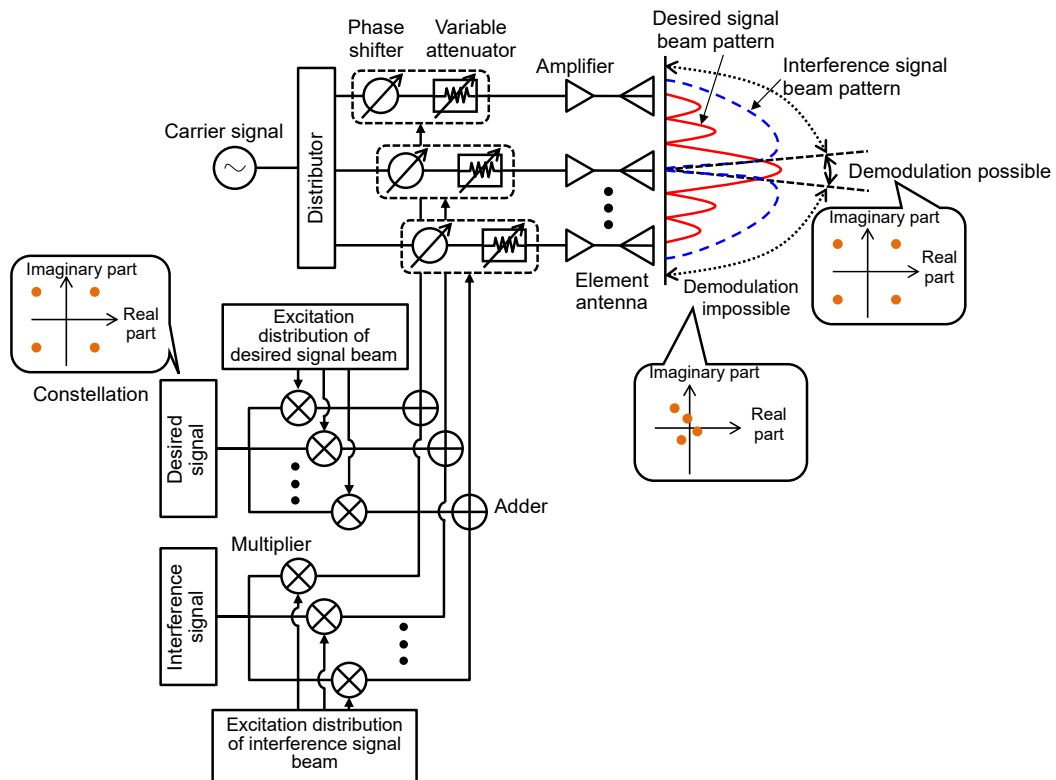


Fig. 2 Configuration of array antenna using directional modulation

3.2 Angle characteristics of bit error ratios

Next, to check how the angular dependence of the constellations affects communication performance, bit error ratio (BER) characteristics in an environment with additive white Gaussian noise were evaluated. Figure 6 shows the BER characteristics when the signal to noise

Table 1 Simulation parameters

Item	Description
Antenna configuration	4 elements, half-wave length interval, linear array antenna
Element antenna	Omnidirectional
Communication direction	Antenna boresight (0-degree direction)
SNR in the communication direction	20 dB
Modulation	QPSK
Interference signal	Phase: 0 degrees

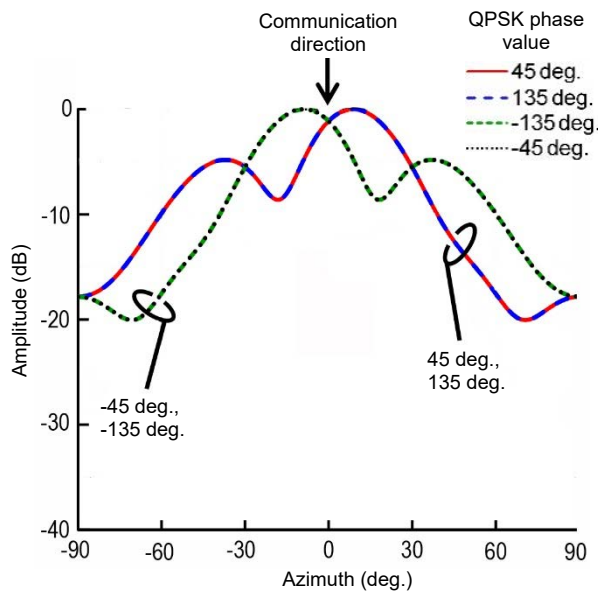


Fig. 3 Far-field amplitude pattern

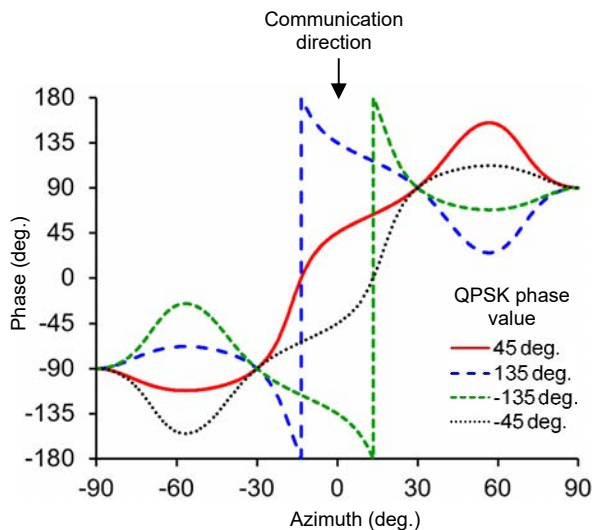


Fig. 4 Far-field phase pattern

power ratio (SNR) in the communication direction (0-degree direction) is 20 dB and the receiving point is changed in a semicircle with a certain distance from the transmitting station. For comparison, the figure also shows the angle characteristics of a conventional array antenna at the time of beam scanning in the communication direction (0-degree direction).

For the conventional array antenna, the SNR at the receiving point changes according to changes in the beam pattern amplitude, so the BER gradually deteriorates as the direction moves away from the communication direction and it becomes local minimum in the direction of the sidelobe peak. The BER improves in the sidelobe direction like this, thus allowing the communication contents to be demodulated even in azimuths other than the communication direction. On the other hand, the figure shows that for the directional modulation array, the BER remains deteriorated in the sidelobe direction of the conventional array antenna and the angle range in which the BER is good can be limited near the communication direction. When the angle width

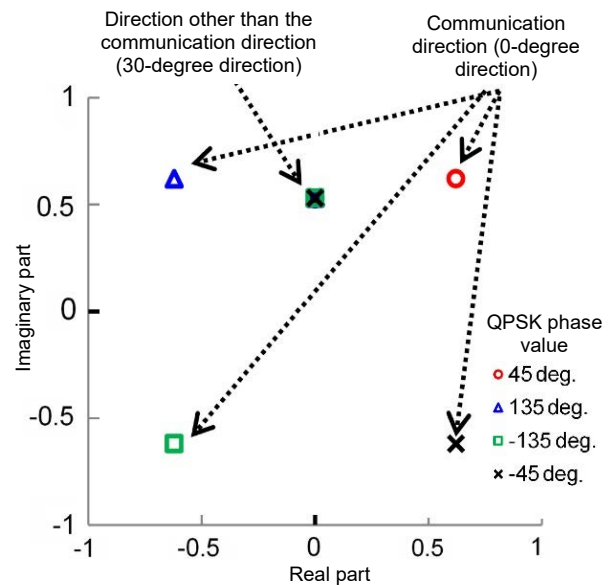


Fig. 5 Constellation diagram of received signal

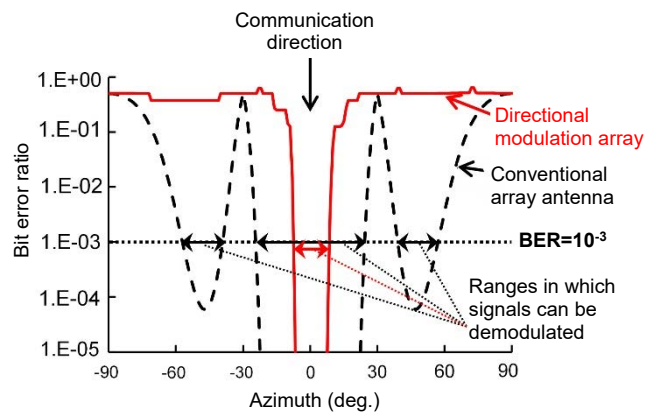


Fig. 6 BER spatial distribution

in which the BER is 10^{-3} or lower is defined as the range in which the contents can be demodulated, the range is 84 degrees for the conventional array antenna and 15 degrees for the directional modulation array. Thus, we have confirmed that using a directional modulation array can limit the range in which contents can be demodulated to approximately one fifth of the conventional value, and that communication is possible only in a limited direction.

4. Conclusion

This paper proposed directional modulation arrays using the sum and difference patterns synthesis method as a technique to limit the range in which contents can be demodulated using phased array antennas and evaluated the communication performance. The results showed that the range in which the contents can be demodulated can be narrowed using this type of antenna compared to conventional array antennas and that communication is possible only in a limited direction. We will study combining this technology with cryptographic techniques in the future, and work to enhance the safety of radio communication systems.

5. References

- (1) Chen, X., et al.: A Survey on Multiple-Antenna Techniques for Physical Layer Security, *IEEE Communications Surveys & Tutorials*, 19, No. 2, 1027–1053 (2017)
- (2) Sasaoka, H.: Information Security at Physical Layer Based on Radio Propagation Characteristics, *IEICE Technical Report*, AP 2015–2021 (2015)
- (3) Daly, M. P., et al.: Directional Modulation Technique for Phased Arrays, *IEEE Transactions on Antennas and Propagation*, 57, No. 9, 2633–2640 (2009)
- (4) Fujimoto, M., et al.: Limited Area Communication Using Sum & Differential Patterns, 2015 International Symposium Antennas and Propagation, 1–2 (2015)
- (5) Kuriyama, et al.: A Study of Limited Communication Area for Directional Modulation Using Active Phased Array Antenna with Sum-Difference Pattern Combining Method, *IEICE Technical Report*, AP 2016-153 (2017)

Multiband Digital Transmitter Techniques Using High-Efficiency GaN Switching-Mode Amplifiers

Authors: *Shintaro Shinjo** and *Rui Ma***

1. Introduction

The size of digital baseband sections on transmitters for wireless installations such as base stations has become smaller and the operation speed has increased as semiconductor processes have become finer. However, it is very difficult to improve the efficiency of high-frequency analog sections including transmitting amplifiers. Therefore, digital transmitter architecture has been attracting attention as the next-generation transmitter architecture. In this architecture, high-frequency signals are processed to digital signals and most of the high-frequency section is operated digitally. The main characteristics of the digital transmitter architecture are as follows: (1) the transmitter is programmable and can be adapted, so it can be easily applied to multiple specifications, (2) the size of the transmitting section can be made smaller by increasing the integration and reducing the number of external parts, and (3) the efficiency can be improved by adopting the switching amplifier circuit architecture.

One main technical challenge for digital transmitters is to develop high-efficiency switching amplifier circuit technology. To use switching amplifiers on transmitters for base stations, they need to have high-efficiency and high-power characteristics in high-frequency bands. Some researchers have recently reported high-efficiency and high-power switching (class D) amplifiers that work in frequency bands near GHz by adopting GaN transistors.^{(1), (2), (3)} This amplifier technology is expected to lead to the development of high-performance multifunction digital transmitters for base stations.

This paper describes multi-band digital outphasing transmitter architecture having switching amplifiers. It also reports on the results of prototyping a two-band digital outphasing transmitter with GaN class-D amplifiers based on the proposed architecture. The efficiency of GaN class-D amplifiers was improved by applying boot-strap driver circuits. In addition, high-efficiency and high-power operation was made possible through class-S outphasing amplification of the two class-D amplifiers by a Chireix power combiner. This type of transmitter showed excellent high-frequency characteristics when sending two frequencies (244 and

500 MHz) at the same time, raising expectations for the development of the new next-generation transmitter architecture using GaN devices.⁽⁴⁾

2. Digital Outphasing Transmitter Architecture for Non-Contiguous Concurrent Multi-Band

Figure 1 shows the block diagram of a multi-band digital outphasing transmitter with the proposed switching amplifiers. This transmitter consists of a signal processing block including a digital signal generator for multi-level (e.g., q level) outphasing that generates signals from digital baseband signals, class-S outphasing amplifying block consisting of class-D amplifiers and a power combiner, and multi-band filter.

The signal processing block converts individual digital baseband signals (I_n and Q_n) to high-frequency signals through digital up-conversion. Then, to enhance the efficiency of signal processing, the multi-band multi-bit bandpass delta-sigma modulation (BPDSM) forms high-linear digital signals in the level of $(2q + 1)$. The digital signal generator for multi-level outphasing forms and outputs two types of q -level digital signals that correspond to the $(2q + 1)$ -level digital signals and that have an outphasing angle.

The two types of digital signals output from the signal processing block are input to each of the two class-D amplifiers constituting the class-S outphasing amplifying block and are amplified. The power combiner combines the amplified signals based on the outphasing angle. The multi-band filter removes harmonic components. The antenna outputs the signals. These processes realize a high-efficiency and high-power digital transmitter that can transmit multi-band signals at the same time.

3. Prototyped Results of Digital Outphasing Transmitter with Two-Dimensional Power Coding

The authors prototyped a two-band digital outphasing transmitter based on the block diagram in Fig. 1. The two frequencies of 244 and 500 MHz were selected. For low-frequency signals, the channel

bandwidth was 5 MHz and the peak-to-average power ratio was 11.0 dB. For high-frequency signals, the channel bandwidth was 10 MHz and the peak-to-average power ratio was 11.7 dB.

3.1 Class-S outphasing amplifier

Figure 2 shows the circuit diagram of the class-S outphasing amplifying block consisting of class-D amplifiers and a Chireix power combiner. The class-D amplifiers have GaN transistors that feature two types of characteristic (high-speed operation and high voltage resistance). They were integrated on a chip as shown in Fig. 3. The chip size is 1.6×0.9 (mm²). A class-D amplifier consists of a switching circuit including two transistors (M_1 and M_2) and driver circuit connected to the gate sides of M_1 and M_2 . The driver circuit of the gate terminal of M_1 , in particular, needs to supply high-voltage amplitude highly efficiently from near the threshold

voltage to the drain voltage (V_{DD}). By applying a bootstrap driver circuit with a capacity for charging and discharging voltage, the circuit can be used under a condition where the drain power supply of the driver circuit on the M_1 side (V_{DDH}) is lower than V_{DD} . As a result, the power consumption of the entire class-D amplifiers can be reduced.

3.2 Digital outphasing transmitter

The authors prototyped a two-band digital outphasing transmitter. Figure 4 is a photograph of the class-S outphasing amplifying block included in the digital outphasing transmitter. Figure 5 shows the results of evaluating the digital outphasing transmitter. The power supply voltage (V_{DD}) of the class-D amplifier was 35 V and the outphasing angle was limited to a range from 0 to 45 degrees. The results of the evaluation were a maximum drain efficiency of 59%, maximum overall

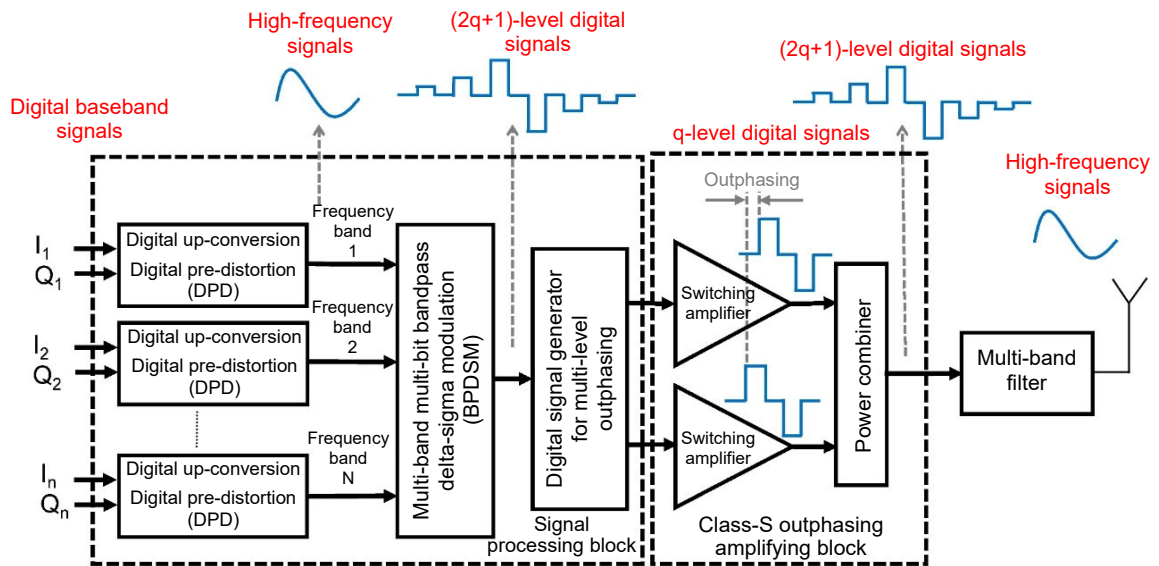


Fig. 1 Architecture of multiband digital outphasing transmitter

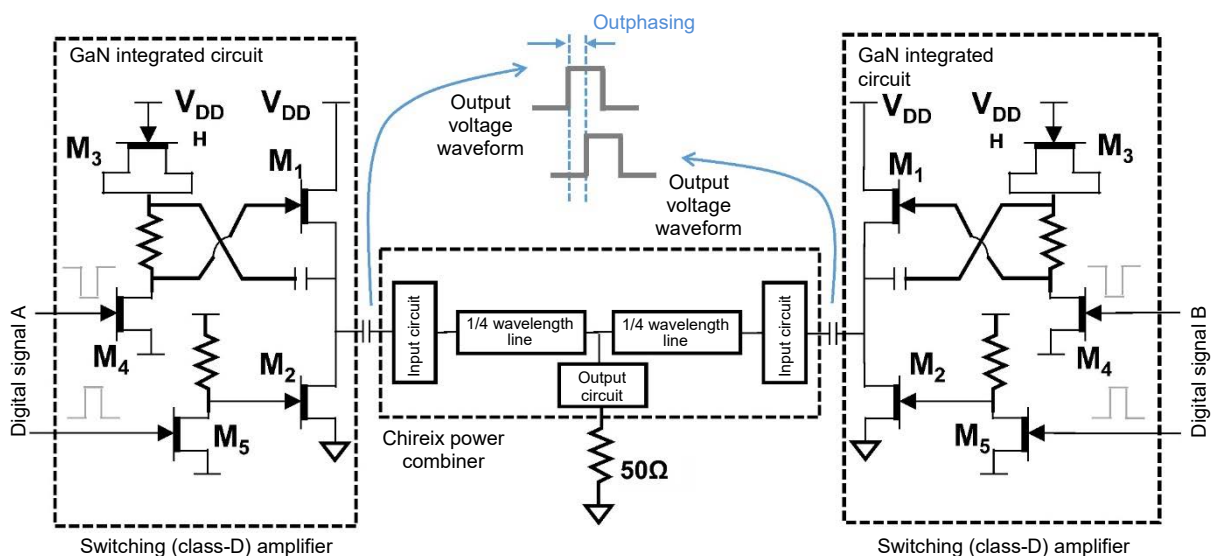


Fig. 2 Circuit of class-S outphasing amplifier block

efficiency of 50%, and maximum output power of 38.0 dBm, thus achieving high efficiency and high power. It has also been confirmed that even when the output power was reduced, the high-efficiency characteristics were retained. Figure 6 shows the results of evaluating the output spectra of the digital outphasing transmitter. Figure 6(a) shows the results when the frequency of the

signals was 244 MHz and the channel bandwidth was 5 MHz. Figure 6(b) shows those when the frequency of the signals was 500 MHz and the channel bandwidth was 10 MHz. The adjacent-channel leaking power for the case in Fig. 6(a) was -37 dBc and that for the case in Fig. 6(b) was -30 dBc. Thus, it has been confirmed that the transmitter has excellent distortion characteristics and can transmit two frequencies at the same time.

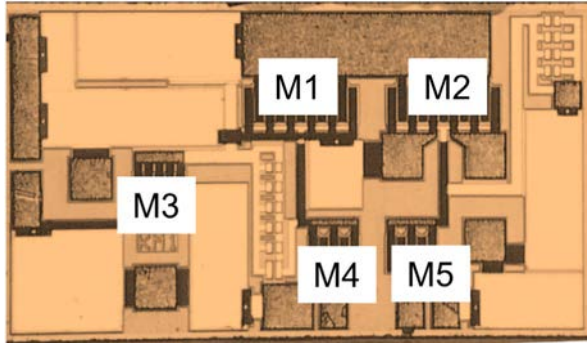


Fig. 3 Chip photograph of GaN switching amplifier

4. Conclusion

This paper reported the results of prototyping a two-band digital outphasing transmitter with class-D amplifiers. The evaluation results show that the transmitter has excellent high-efficiency and high-power characteristics and that the architecture is effective for digital transmitters for base stations that will require higher efficiency and more functions in the future. The results also indicate the potential for developing new GaN devices.

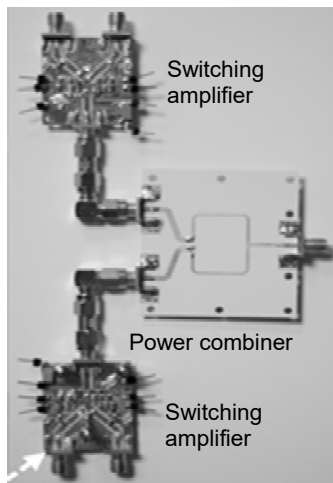
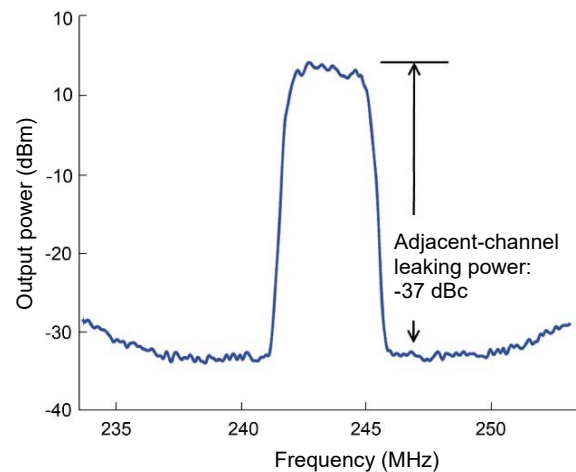


Fig. 4 Prototyped class-S outphasing amplifier block



(a) 244 MHz frequency, 5 MHz channel bandwidth

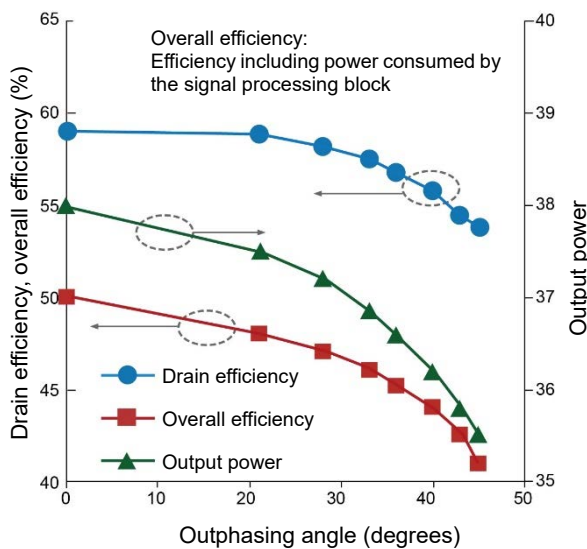
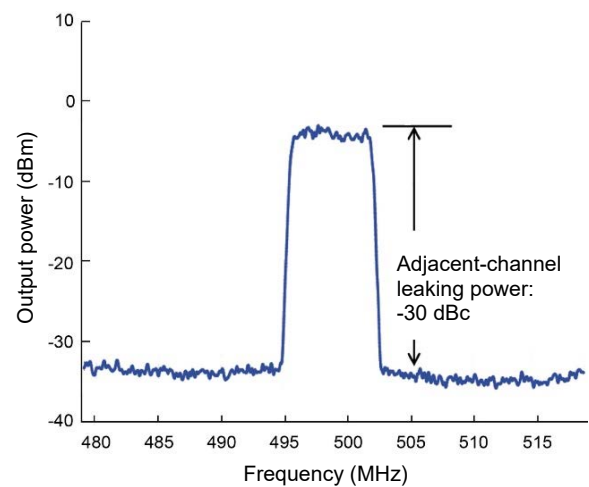


Fig. 5 Measured results of digital outphasing transmitter



(b) 500 MHz frequency, 10 MHz channel bandwidth

Fig. 6 Measured output spectrum of digital outphasing transmitter

5. References

- (1) Hori, S., et al.: Linear and Efficient Digital Transmitters for Future Mobile Communication, IEEE International Microwave Symp. Workshop (2017)
- (2) Andreas, W., et al.: Digital Transmitters for the Wireless Infrastructure, IEEE International Microwave Symp. Workshop (2017)
- (3) Nakamizo, H., et al.: Over 65% PAE GaN Voltage-Mode Class D Power Amplifier for 465 MHz Operation Using Bootstrap Drive, IEEE Radio Wireless Symp. (2015)
- (4) Sung, W. C., et al.: Concurrent Multiband Digital Outphasing Transmitter Architecture Using Multidimensional Power Coding, IEEE Trans. Microw. Theory Tech., Vol. 63, 598–613 (2015)

